PCMDI

Program for Climate Model Diagnosis and Intercomparison

UCRL-ID-121413

PCMDI Report No. 23

INTERCOMPARISON OF THE SPECTRAL CHARACTERISTICS OF 200 hPa KINETIC ENERGY IN SOME AMIP SIMULATIONS

by

James S. Boyle

Program for Climate Model Diagnosis and Intercomparison
Lawrence Livermore National Laboratory, Livermore, CA, USA

July 1995

PROGRAM FOR CLIMATE MODEL DIAGNOSIS AND INTERCOMPARISON
UNIVERSITY OF CALIFORNIA, LAWRENCE LIVERMORE NATIONAL LABORATORY
LIVERMORE, CA 94550

INTERCOMPARISON OF THE SPECTRAL CHARACTERISTICS OF 200 hPa KINETIC ENERGY IN SOME AMIP SIMULATIONS

James S. Boyle

Program for Climate Model Diagnosis and Intercomparison
Lawrence Livermore National Laboratory
Livermore, CA, USA

ABSTRACT

The 200 hPa kinetic energy budget terms are represented by means of their spherical harmonic components for a number of AMIP simulations. The data used are the monthly mean wind fields for 1979 to 1988 decadal simulations. The budget terms are decomposed into the divergent and rotational components. The comparison is limited to the lower wavenumbers so as to be within the nominal limits imposed by the models with the coarsest spatial resolution.

The results show considerable differences among the models. The comparison is best for the rotational wind and degrades for the divergent components, especially the conversion term. There is some ambiguity among the models as to the sign of some terms at certain wavenumbers. The models tend to overestimate the Walker type (east-west) divergent circulations compared to the Hadley type (north-south) compared to recent NMC and ECMWF operational analyses.

The inter-model differences are substantial when viewed in light of the differences in the observational analyses and ensemble differences for the ECMWF model. However, the median values of all the models taken together are usually in fair agreement with observational values.

There is no obvious, systematic pattern of errors which can be consistently attributed to specifics of the individual model horizontal and vertical resolution, numerics or physical parameterizations.

1. Introduction

Kinetic energy has long been regarded as a fundamental property of the atmospheric general circulation. In the historic work of Lorenz (1955), kinetic energy was the measure of the atmospheric motion. Since Lorenz there have been many variations on the global energy cycle. There exist a near infinite number of ways to decompose the various components of the atmospheric circulation in the space and time domains. The choice of the decomposition is largely determined by the purpose of the analysis. In the present context the object is to intercompare the properties of the kinetic energy at 200 hPa for a number of ten year GCM climate simulations. The 25 models have a wide variation in numerics, spatial resolution and physical parmeterizations. The goal of this work is to gain some insight into the nature of the model differences and perhaps ambitiously, their causes. To this end, we chose to decompose the kinetic energy into its rotational and divergent components in the space of spherical harmonics.

The division of kinetic energy into the rotational and divergent components provides more information on the nature of the dynamics than by looking at the total kinetic energy. The divergent flow is intimately connected to the generation of kinetic energy by the secondary circulations and is closely linked with the diabatic forcing. Thus it can be used as an indicator of the forcing by these processes as parameterized in the models. The effects of the various parameterization choices among the models considered is of prime interest.

The spherical harmonic decomposition has proved to be useful in past work. Lambert (1984, 1987) has performed a comprehensive analysis of observed data and output from the Canadian Climate Centre GCM (This model is an earlier version of the CCC model cited in this work). He found that the model did a good job in qualitatively simulating the kinetic energy budget but some the magnitudes of the energies and conversions at some wavenumbers were not well represented in the simulation. The decomposition into spectral space will provide some measure of the scale dependency which might provide some insight as to the effects of the horizontal resolutions of the models.

The intent here is not a contest to determine the "best" model. Rather, this work should be seen as a summary of the state of modeling the atmosphere from a rather narrow perspective. the results will show that a consensus among models has not

been achieved. More development is evidently required to simulate the atmospheric component of the climate system with complete fidelity.

2. Computational Formulation

In order to be clear in terminology, the equations for transforming to spherical harmonics will be presented. A arbitrary variable x distributed in latitude (ϕ) and longitude (λ) can be expressed in terms of spherical harmonics as follows:

$$x(\lambda,\phi) = \sum_{n=0}^{N} \sum_{m=-n}^{n} X_n^m P_n^m(\sin\phi)\, e^{im\lambda}$$

where:

$$X_n^m = \frac{1}{2\pi}\int_0^{2\pi} x(\lambda,\phi)\, P_n^m(\sin\phi)\cos(\phi)\, e^{-im\lambda}\, d\phi d\lambda$$

and where P_n^m is the associated Legendre polynomial of the first kind of order m and degree n, X_n^m is a coefficient of the spherical harmonic representation of x, and N is the limiting wavenumber of the triangular truncation.

The equations for kinetic energy is spherical harmonics follow the procedures of Lambert (1984, 1990). The decomposition is done in terms of spherical harmonics of order m and degree n. The equations for the divergent and rotational components of the kinetic energy as derived by Lambert are:

$$\frac{\partial}{\partial t}\mathrm{rotK}_n^m = \mathrm{rotL}_n^m + \mathrm{rotF}_n^m - \mathrm{rot}\Delta_n^m \qquad (1)$$

$$\frac{\partial}{\partial t}\mathrm{divK}_n^m = \mathrm{divL}_n^m + \mathrm{divF}_n^m + C_n^m + \mathrm{div}\Delta_n^m \qquad (2)$$

In (1) the rotK_n^m term represents the rotational kinetic energy, The rotL_n^m is the conversion of divKE in all modes and all wavenumbers to rotKE in mode (m, n) and transfer of rotKE from all modes and wavnumbers to mode (m,n), rotF_n^m is a conversion of divergent KE to rotational KE resulting from interactions involving the Co-

riolis terms. This term is responsible for a conversion of divergent KE in modes (m, n-1) and (m, n−1) to rotational KE in mode (m,n). The $rot\Delta_n^m$ term represents the dissipation of rotational KE.

In (2) the $divK_n^m$ term represents the divergent kinetic energy, C_n^m describes the conversion of available potential energy (APE) to divergent KE. The $divL_n^m$ is the conversion of rotKE in all modes and all wavenumbers to divKE in mode (m, n) and transfer of divKE from all modes and wavnumbers to mode (m,n), $divF_n^m$ is a conversion of rotational KE to divergent KE resulting from interactions involving the Coriolis terms. This term is responsible for a conversion of rotational KE in modes (m, n-1) and (m, n+1) to divergent KE in mode (m,n). The $div\Delta_n^m$ term represents the dissipation divergent KE.

Figure 1, which is after Lambert (1990), is a schematic of the KE budget expressed in (1) and (2). The coupling between the rotational and divergent budgets are by the F_n^m and L_n^m terms. Studies by Chen and Winn-Nielsen (1976), and Lambert (1990) showed that the F_n^m terms account for most of the divergent - rotational KE exchanges.

As explained in the next section the data available do not permit the computation of the L_n^m terms nevertheless the remaining components do provide and interesting picture of the dynamics of the models.

The question of the nature of the truncation arises when dealing with the representation of fields in terms of series of spherical harmonics. The models varied in their horizontal representations. Some were gridpoint models, the rest used a spherical harmonic representation with either a triangular (T) or rhomboidal (R) truncation. In an attempt to be as even handed as possible for all the models, the calculations were carried out in the spherical harmonic space that is appropriate for each model. For the grid point models and the gridded observational data, a triangular truncation was chosen commensurate with the number of nodes from pole to pole. For the models cast in the spherical harmonics framework the calculations were carried out in the appropriate spectral space. The results are presented for portions of the spectra where any computational artifacts generated by these differences in representation and choices of truncation should be minimal.

Many of the results will be given in terms of the two dimensional wavenumber n. This method of presentation was originally advocated by Baer (1972) and has proved useful in the work of Baer (19742, Lambert(1984), and Boer and Shepherd(1983). In order to obtain results solely in terms of the two-dimensional wavenumber, n, it is required to sum over the order m for each n.

3. Data

The Atmospheric Model Intercomparison Project (AMIP) of the World Climate Research Programme's Working Group on Numerical Experimentation (WGNE) permits some insights as to the general nature of the model GCM response to SST variations. The participants in AMIP simulate the global atmosphere for the decade 1979 to 1988 using a common solar constant, and CO2 concentration, and a common monthly averaged SST. and sea ice data set. An overview of AMIP is provided by Gates (1992). The AMIP experiment will allow some assessment of the extent to which the models have a common low frequency response to the identical external forcing of the SST variations.

The AMIP models used in this study are identified in Table 1 and their horizontal and vertical resolutions are shown. As important as the spatial configuration of the model are the parameterizations used to simulate moist convective heating, fluxes of heat, moisture and momentum, precipitation, clouds and so forth. The complete specifications of the parameterizations used in the models are described in Philips (1994). The various penetrative convective parameterizations are probably crucial elements in the simulations but it is difficult to succinctly characterize them. For a specific scheme, say the Kuo scheme, there are so many variations and critical differences in implementations that simply identifying a parameterization by the single nomenclature can be misleading.

The wind and geopotential height data from the AMIP simulations was only available for the 200 and 850 hPa levels and the vertical motion field was not archived. The terms for (1) and (2) were computed for the for the 200 hPa level only. The problems with the 850 hPa level is that the extrapolation method below the surface was not uniform across the models and some groups chose not to perform the extrapolation at all. Since the focus of this study was to clearly establish model differences it was felt that only the terms at 200 hPa would be computed, since these are not as

strongly influenced by the somewhat arbitrary post-processing procedures used to obtain pressure level data. In any case the L_n^m terms cannot be computed since they involve vertical motion. The dissipation terms, which are most often computed as a residual, cannot be computed either.

In other studies, Lambert(1984, 1987) , Burrows (1976), Bauer (1972), Boer and Shepherd (1983) , the KE budgets are carried out for vertically integrated data. It must be emphasized that caution must be used in any comparison of the results here to the studies using vertically integrated terms. As is well known, the correspondence of the conversion term, C_n^m in the KE and APE budgets is only for the vertically integrated quantities. All that can be done with the data in hand is to compute the single level contribution to the integral. The work of Boer and Shepherd (1983) indicates that the 200 hPa level is the most active in the KE budget, and thus the terms computed at this level will be important if not dominant in the total KE budget. This implies that differences in the model simulations at this level will be a substantive yardstick of relative model performance.

The observed data available was that of the operational analyses of the ECMWF and NMC. The ECMWF data was for the period 1980 to 1989, the NMC data matched the simulations in that the 1979 to 1989 decade was available. The shortcomings of the operational analyses of the ECMWF and NMC in regards to the divergent component of the wind are well documented, Trenberth and Olsen (1988, 1988a), Lambert (1989) The consensus opinion of the studies is that the operational analysis had significant problems for the better part of the 1979 to 1988 decade. In light of these studies the observational data computations were limited to the period 1986 to 1989. Although the data for this period are deemed more reliable, they are for a somewhat shorter period than the model simulations. It was felt that to obtain reliable statistics for model intercomparison the full decade of model data should be used while for the sake of accuracy the time truncated observational set be used as an estimate of likely values for the various terms.

4. Results

a. KE spectra

Figure 2 presents the two-dimensional wavenumber spectra of the rotational

and divergent kinetic energy for all the models (averaged from 1979 to 1988) and observations(averaged from 1986 to 1989) for the solstitial seasons. The data of this figure and subsequent spectra are restricted to two dimensional wavenumbers n < 15. This range is consistent with all the models to be displayed since it is within the resolution of all the models even those with the coarsest horizontal resolution.

The vast bulk of the kinetic energy for the 200 hPa windfield is contained in the rotational component. The shape of the spectra of the rotational kinetic energy components of the models are generally in agreement with each other and the observations, especially at the lower wavenumbers(n < 7). The good agreement between the two sets of observations gives some confidence in the ability of the analysis to accurately depict this spectrum. The spectra of the observational data agree rather well with the vertically integrated results of Boer and Shepherd (1983) and Lambert(1987, 1984). The tendency for the peaks in the rotational KE to occur at odd n is due to the fact that the contribution of the symmetric zonal wind to the rotational component is to the odd n, Lambert (1987).

Comparing Figs. 2a and 2b, there is a marked increase in the energy at wavenumber 2 in going from DJF to JJA and a drop in energy in wavenumber 1. This behavior was documented in the with data from the FGGE year by Boer and Shepherd (1983). It is consistently simulated by the models.

Although all the models generally follow the variations of the observational data with wavenumber, there is a considerable range in the actual values. Keep in mind that this is a log plot, the extreme variations amongst the models for wavenumber 1 in JJA amounts to almost a factor of 10. The amplitude at n = 1 is an indicator of the Equator to pole temperature gradient. Lambert (1987) comments that the tendency for the poles to be too cold in the model he analyzed is reflected in an overestimate of the rotational KE at n = 1. Here there seems to be a tendency for the models to underestimate the n=1 values in DJF but for both seasons the models are scattered about the observational value. In JJA there is not a model consensus on the dominant wavenumber between 1 and 2. Some wavenumbers have consistent overestimates, e.g. n = 5 in JJA, and others are underestimated, e.g. n=2 in DJF.

The divergent KE spectra in Figs. 2c and 2d show a large variation in going from DJF to JJA but no single wavenumber stands out as did n =2 for the rotational KE. The divergent KE tend to have a larger spread between the observational data sets, although this difference is generally less than the range amongst the models.

Figure 3 presents the spectra for the conversion, rotF and divF terms for the solstitial seasons. Note that these are presented on a linear plot. Overall, the models capture the sense of the transitions between the seasons and the general shape and magnitude of the spectra. Nevertheless, there are significant differences. The models have differences from each other and the observations which often exceed the uncertainty represented by the observational disagreement. There are instances where the models and observations differ in sign, and places where the observations have extrema of the opposite sense to some of the models.

In the DJF conversion term, Fig. 3a, there is not agreement as to the sign of this term for n = 2. In the JJA plot, Fig. 3b, all the models capture the large increase at n = 1 in going from DJF to JJA but the models have considerable disagreement on the magnitude of the JJA value. The models have relatively more success in the transition in going from DJF to JJA at n = 6.

The divF term in Figs. 3c and 3d show much the same problems as the conversion term. There is a tendency of the models to overestimate this term at n = 5 with the models displaying more seasonal variation at this wavenumber than the observations. The divF term tends to mirror the variations of the conversion term. The was observed for the vertically integrated budget by Lambert (1987). This is a reflection of the fact that the main balance in (2) is between divF and conversion. The rotF term, Figs. 3e and f, has less of a seasonal change than its divergent counterpart. There is a wide variation in the values at n = 1, with no model consensus on the sign of this term. The prominent values at n = 3 are probably the result of the stationary wave pattern which has a large signature at this scale.

b. KE in M/N space

The spectra in the foregoing figures show the data collapsed to a single wavenumber. This compaction is useful for the presentation of the results from such a large number of models. However, as pointed out by Baer (1972), an insightful plot is to contour the values of the spectral data in the space of m and n-m. This yields another degree of dimensionality, so that only select plots can be shown but allows further insight as to the spectral disposition of the data.

Plots of the ECMWF observed rotational and divergent kinetic energy, rotF, divF and Conversion are given in Figs. 4 and 5. The values of n-m (the number of north south nodes) are along the ordinate, the zonal wavenumber m (the number of east

west nodes) form the abscissa. A summation taken along a diagonal from the ordinate axes (m = 0) to the abscissa (n-m= 0) corresponds to the values shown in Figs. 2 through 3.

Figures 4a.b presents the spectral decomposition for the ECMWF analyses for the divergent and rotational wind for DJF. Note that the contour interval is approximately logarithmic. The data for the NMC analysis are generally in good agreement with those of the ECMWF. Comparing the rotational KE and divergent KE, it is apparent that the rotational KE is confined to the m = 0 modes, while the divergent KE tends to be more isotropic with maxima along both the m = 0 and n-m = 0 axes. This is a reflection of the dominance of the zonal wind in the rotational component. Baer (1972) displayed similar plots for the zonal and meridional KE and these resemble the plots for the rotational and divergent KE, respectively. Even for the divergent KE the components on the two axes dominate any contribution from the interior. Note that the contour interval is logarithmic, so the appearance of Figs. 4b and 5b can be misleading. All the models have plots which resemble Fig. 4, with variations consistent with the data in Figs. 2 and 3.

In the DJF kinetic energy plots, Figs. 4a and 4b, there is a maxima at m,n = (3,6). This is probably due to the stationary wave pattern which is strongest during the northern winter. This is a feature common to all the models, although varying in magnitude. It is commonly thought that the stationary waves at this scale are forced by both orographic effects and longitudinal variations in heating, e. g. Hoskins and Pearce (1973). It would seem that the model horizontal resolution would have some impact on its ability to simulate these features commensurate with the ability to depict the orographic details. However, a comparison of the magnitudes of the KE at (m,n) = (3,6) did not reveal any consistent tendency as a function of either horizontal or vertical resolution.

The fact that most of the energy is distributed along the axes for the divergent KE suggests a way of reducing the complexity of the spectral decomposition by simply adding up the modes along each axis and plotting the sums as a scatter diagram for all the models. This is appropriate only for the divergent KE since the others are overwhelmingly dominated by the m = 0 axis, and thus the spectra using n (Figs 2 to 3) are more than adequate to describe the distribution. For the divergent flow the m = 0 (no nodes along a line of constant latitude) modes can be interpreted as a Hadley / Ferrell type north south oriented circulation. The n -m = 0 (no nodes along a line of

constant longitude) represents an east-west or Walker type of flow. Figure 6 is a Tukey sum difference plot, Cleveland (1985), where the ordinate has the difference of the Σ[divergent KE (n=0)] - Σ[divergent KE (m = 0)] and the abscissa is the sum. This type of plot is designed to facilitate assessment of any biases in the data and their magnitudes. Figure 6 indicates that the models have a marked tendency to overestimate the east-west divergent flow with respect to the north-south circulation, especially during the northern summer. On the other hand, the figures also show that the models are fairly evenly distributed about the observed total divergent KE. In order to get a better feel for the kinds of flow differences that these biases represent, the velocity potential will be plotted for three specific models for the JJA season. The models chosen are the CNR , UGA and ECM. All these models have the same horizontal resolution, T42. They all have roughly the same total divKE value and represent two extreme cases, UGA and CNR, with the ECM nearer to the observed ratio. It is also of interest that the UGA and ECM are both very close in model formulation, the UGA model being derived originally from the ECM code. The major difference is that the UGA uses the Betts Miller convective scheme, Slingo et al. (1994) and the ECM uses a mass flux scheme of Tiedtke(1989). Comparing the extreme cases of UGA and CNR, Figs. 7c and 7b respectively, the dominance of the Walker type circulation in the CNR flow compared to the Hadley circulation in the UGA field is quite plain. The ECM and UGA are clearly in closer agreement. The difference in the convective parameterization leads to an ITCZ that is more prominent in the UGA model as compared to the ECM. However, it should be noted that there is no apparent overall direct relation between penetrative convective schemes and the position on Fig. 6 . For example GFD, BMR and GLA join CNR on the extreme side of Fig, 6b but their convective schemes are moist convective adjustment, a Kuo derivative and a mass flux scheme, respectively. Phillips (1994) can be used for the specific details on the parameterizations.

The point is that the models behave in a rather different fashion from each other for this critical portion of the general circulation. Even if the observed values shown in Fig. 6 are subject to error, there is little evidence of a consensus from the models. The lack of agreement on the character of the divergent flow is a sensitive indicator that the models must further work on the suite of parameterizations. Some evidence points to the convective parameterization as a critical element but it appears as if the synergy of all the various physical processes must be improved to get a reliable cli-

mate sensitivity.

5. Discussion and Conclusions

The spectra of Figs. 2 and 3 which include all the models are overwhelming in their complexity. The point of the figures is not to carefully track the performance of individual models but to provide a sense of the consensus picture of the models. In this section an attempt will be made to make a more quantitative assessment of the distribution of model values for the various quantities in the KE budget. The boxplot, Cleveland (1985), has been long used in statistics to graphically portray the statistical distribution underlying a number of samples. Figures 8 and 9 contain the same data as a boxplot for the KE budgets. At each value of n are plotted the extreme values, the 25th the 75th percentiles, the 90th and 10th percentiles and the median (50th percentile value) of the data from all the models. Also plotted are curves for the NMC and ECMWF analyses. The median should be a fairly robust estimate of the overall skill of the models in estimating the parameter considered.

A positive feature of Figs. 8 and 9 is that for many of the variables, especially the rotational and divergent KE, the median value for the models is close to that of the observations. Although the spread of the values can be disheartening, the consistent accuracy of the median for variables where the observations are reliable indicates that the model parameterizations are capturing the majority of the forcing for these variables.

The DJF rotational KE , Fig. 8a, shows a consistent underestimate by the models compared to observations for n = 2. The observational data falls at the 90th percentile level for the models. The rotF term for DJF, Fig. 8c, has the observational estimate at above the 90th percentile at n = 2. The models have a large range for this wavenumber, but the observations are in good agreement with each other. There is a considerable spread for both the observations and models at n = 3. This extrema in the curve is probably due to the stationary wave components and the results in Fig. 8c indicate considerable uncertainty. The DJF divF data, Fig. 8d, show that the models do poorly for the minima at n = 2, but do rather well for the large peak at n = 6. The conversion term, Fig. 8e, follows the divF tendencies.

The JJA data, Fig. 9, show good agreement with respect to the median. The good agreement with observations by the divergent KE, Fig. 9b, must be tempered by the

substantial discrepancies in the distribution in the two dimensional wavenumber space shown in Fig. 6. The rotF, divF and conversion terms for JJA, Fig. 9c, d, e, represent the most severe shortcomings of the models. The problems are egregious at the lowest wavenumbers and are no doubt linked to the biases in the flow shown in Fig. 6.

For the purpose of comparison to past work the total F terms for both seasons are shown in Fig. 10. These data are the sum of divF and rotF and can be compared to the data of Lambert(1987) since he did not decompose the terms into the two components. The shape of the curves is quite close in comparison to Lambert (1987) although his results were for the vertically integrated quantities. The only difference is at n = 3, where Fig. 10a has a large peak and Lambert's data is near zero. This is probably due to the substantial contribution from the stationary wave pattern at 200 hPa, which is somewhat reduced at the lower levels. It should be noted that the totF values are for the most part in better agreement with the observations than the individual terms. This is especially true for JJA at the lower values of n. There is evidently some compensation in the models in maintaining a total energy exchange among the waves at near the observed values. The complementary nature of the totF and conversions terms indicate that energy is extracted from the large scale (n very small) direct circulations to provide a source of energy to drive the indirect circulations which are situated at the higher wavenumbers.

c. Sensitivity

One way to put these differences and distributions in perspective is to compare them to the uncertainty in the observations represented by the differences in the NMC and ECMWF analyses. The models generally have a greater variation amongst themselves than this difference. However, the integrations represented here are only single realizations of each models simulation. Another way to gauge the how meaningful the variations of the models are is the compare them to the variations between multiple realizations of the models. To this end five decadal realizations of the ecm model were analyzed and some representative results are shown in Fig. 11. The realizations differed only in the initial conditions, the initial conditions for runs subsequent to the first were taken from the end of the previous run. The same AMIP SST data set was used for each integration. Figure 11 shows the JJA divKE and conversion terms. These spectra are robust across the realizations for this model. The diagram analogous to Fig.6 for the different realizations indicates that this aspect is also faithfully reproduced for all members of the ensemble. The implication is that the dif-

ferences amongst the models are not just due to sampling errors but represent fundamental differences in the nature of the windfields at 200 hPa if the ECMWF model is representative of typical model sensitivity.

Acknowledgments. The cooperation of the ECMWF in making their forecast model available and in providing expert technical advice for this research is gratefully acknowledged. The generosity of the modeling groups involved in AMIP in making their results available is greatly appreciated. This work was performed under the auspices of the Department of Energy Environmental Sciences Division by the Lawrence Livermore National Laboratory under contract W-7405-ENG-48.

6. References

Baer, F., 1972: An alternate scale representation of atmospheric energy spectra. *J. Atmos. Sci.*, **29**, 649-664.

Boer, G. J. and T. G. Shepherd, 1983: Large-scale two-dimensional turbulence in the atmosphere. *J. Atmos. Sci.*, **40**, 164-184.

Burrows, W., 1976: A diagnostic study of atmospheric spectral kinetic energetics. *J. Amos. Sci.*, **33**, 2308-2321.

Chen, T.-C. and A. Winn-Nielsen, 1976: On the kinetic energy of the divergent and nondivergent flows in the atmosphere., *Tellus*, **28**, 486-498.

Chen, T.-C. and A. Winn-Nielsen, 1978: On nonlinear cascades of atmospheric energy and enstrophy in a two-dimensional index., *Tellus*, **30**, 313-332.

Cleveland, W. S., 1985 : *The Elements of Graphing Data*, Wadsworth Advanced Books and Software, Monterey, CA, 323pp.

Hoskins, B. J. and Pearce, R., 1973: *Large Scale Dynamical Processes in the Atmosphere*, Academic Press, New York 397pp.

Lambert, S. J., 1984: A global available potential energy-kinetic energy budget in terms of the two-dimensional wavenumber for the FGGE year. *Atmos.-Ocean*, **22**, 265-282.

Lambert, S. J., 1987: Spectral energetics of the Canadian Climate Centre general circulation model., *Mon. Wea. Rev.*, **115**, 1295-1304.

Lambert, S. J., 1989: A comparison of divergent winds from the National Meteorological Center and the European Centre foe Medium Range Forecasts global analyses for 1980-1986. *Mon. Wea. Rev.*, **117**, 995-1001.

Lambert, S. J., 1990: Observed and simulated intraseasonal energetics. *J. Clim.*, **3**, 1330-1346.

Lorenz, E. N., 1955: Available potential energy and the maintenance of the general circulation., *Tellus*, **7**, 157-167.

Phillips, T. J., 1994: A summary documentation of the AMIP models. PCMDI Report No. 18, Program for Climate Model Diagnosis and Intercomparison, University of California, Lawrence Livermore National Laboratory, Livermore, CA, 343pp.

Slingo, J., Blackburn, M., Betts, A., Brugge, R., Hodges, K., Hoskins, B., Miller, M., Steenman-Clark, L., and Thuburn, J. 1994: Mean climate and transience in the tropics of the UGAMP GCM: Sensitivity to convective parameterization. *Q. J. R.*

Meteor. Soc., **120**. 881-922.

Tiedtke, M., 1989: A comprehensive mass flux scheme for cumulus parameterization in large scale models., *Mon. Wea. Rev.*, **117**, 1779-1800.

Trenberth, K. E. and J. G. Olson, 1988: *Evaluation of NMC Global Analysis: 1979-1987*. NCAR/TN-299+STR, Climate and Global Dynamics Division, NCAR, Boulder, CO 82pp.

Trenberth, K. E., and J. G. Olsen, 1988a: *A Comparison between NMC and ECMWF global analyses: 1980-1986*. NCAR/TN-301+STR,Climate and Global Dynamics Division, NCAR, Boulder, CO 96pp.

7. Figure Captions

Figure 1. Schematic of the divergent rotational kinetic energy budget (After Lambert, 1990). Notation is explained in the text.

Figure 2. Rotational kinetic energy spectra at 200 hPa for all the models and the observations for (a) DJF and (b) JJA. (c) and (d) as in (a) and (b) only for the divergent kinetic energy. The ordinate is the two dimensional wavenumber n, described in the text.

Figure 3. Contribution to the conversion term of the kinetic energy budget at 200 hPa for all the models and the observations for (a) DJF and (b) JJA. (c) and (d) as in (a) and (b) except for the divF term (described in text). (e) and (f) as in (a) and (b) except for the rotF term (described in text).

Figure 4. The terms of the kinetic energy budget for the ECMWF analysis for DJF displayed in full spherical harmonic space. The ordinate is the number of north south nodes, the abscissa is the east west nodes. (a) Rotational kinetic energy (J/kg), (b) Divergent kinetic energy (J/kg), (c) rotF (W/kg), (d) divF (W/kg), (e) conversion term (W/kg). The contour interval is approximately logarithmic.

Figure 5. As in Figure 4. except for JJA.

Figure 6. A Tukey sum-difference plot for the $\Sigma(m=0)$ and $\Sigma(n-m=0)$ modes of the 200 hPa divergent kinetic energy for all the models and observations.

Figure 7. (a) The decadal JJA mean 200 hPa velocity potential for the ecm model. The contour interval is 0.5×10^6 m2/sec. Solid lines are zero or positive values, negative lines are negative. (b) as in (a) except for the cnr model. (c) and in (a) except for the uga model.

Figure 8. A statistical summary spectra of the 200 hPa kinetic energy budget for DJF. Displayed are the 10th, 25th, 50th(median), 75th and 90th percentile values computed among all the models for each n. Also shown are the extreme values from the models. For reference the NMC and ECMWF data are also plotted. (a) Rotational kinetic energy, (b) divergent kinetic energy, (c) rotF, (d) divF, (e) conversion term.

Figure 9. As in Fig. 8 except for the JJA season.

Figure 10. (a) As in Fig. 8 except for the total F terms (divf + rotF). As in (a) except for JJA.

Figure 11. (a) The divergent kinetic energy spectra at 200 hPa for an ensemble of five AMIP simula-

tions using the ECMWF model. Also plotted are the ECMWF and NMC observed values. (b) As in (a) except for the conversion term.

8. Table Captions

Table 1. Models used in this study and some aspects of their spatial resolution. Table taken from Phillips (1994). See Phillips for a comprehensive description of each model.

Table 1.

AMIP Model	Horizontal		Vertical		
	Representation	Resolution	Coordinates	No. Levels	Bottom, Top
BMRC	spectral	rhomboidal 31	sigma	9 (3, 3)	991. 9 hPa
CCC	spectral	triangular 32	hybrid	10 (3, 4)	980. 5 hPa
CNRM	spectral	triangular 42	hybrid	30 (4, 20)	995. 0.01 hPa
COLA	spectral	rhomboidal 40	sigma	18 (5, 4)	995. 10 hPa
CSIRO	spectral	rhomboidal 21	sigma	9 (3, 3)	979. 21 hPa
CSU	finite difference	4 x 5 degrees	modified sigma	17 (2, 6)	variable. 51 hPa
DERF	spectral	triangular 42	sigma	18 (5, 5)	998. 2 hPa
DNM	finite difference	4 x 5 degrees	sigma	7 (1, 1)	929. 71 hPa
ECMWF	spectral	triangular 42	hybrid	19 (5, 7)	996. 10 hPa
GFDL	spectral	rhomboidal 30	sigma	14 (4, 4)	997. 15 hPa
GISS	finite difference	4 x 5 degrees	sigma	9 (2, 2)	975. 10 hPa
GLA	finite difference	4 x 5 degrees	sigma	17 (5, 4)	994. 12 hPa
GSFC	finite difference	4 x 5 degrees	sigma	20 (5, 7)	994. 10 hPa
JMA	spectral	triangular 42	hybrid	21 (6, 7)	995. 10 hPa
LMD	finite difference	50 sinlat x 64 lon	sigma	11 (3, 2)	979. 4 hPa
MGO	spectral	triangular 30	sigma	14 (5, 4)	992. 13 hPa
MPI	spectral	triangular 42	hybrid	19 (5, 7)	996. 10 hPa
MRI	finite difference	4 x 5 degrees	hybrid	15 (1, 9)	variable. 1 hPa
NCAR	spectral	triangular 42	hybrid	18 (4, 7)	992. 3 hPa
NMC	spectral	triangular 40	sigma	18 (5, 4)	995. 21 hPa
NRL	spectral	triangular 47	hybrid	18 (5, 5)	995. 1 hPa
SUNYA	spectral	rhomboidal 15	sigma	12 (3, 5)	991. 9 hPa
UCLA	finite difference	4 x 5 degrees	modified sigma	15 (2, 9)	variable. 1 hPa
UGAMP	spectral	triangular 42	hybrid	19 (5, 7)	996. 10 hPa
UIUC	finite difference	4 x 5 degrees	sigma	7 (3, 0)	990. 200 hPa
UKMO	finite difference	2.5 x 3.75 degrees	hybrid	19 (4, 7)	997. 5 hPa

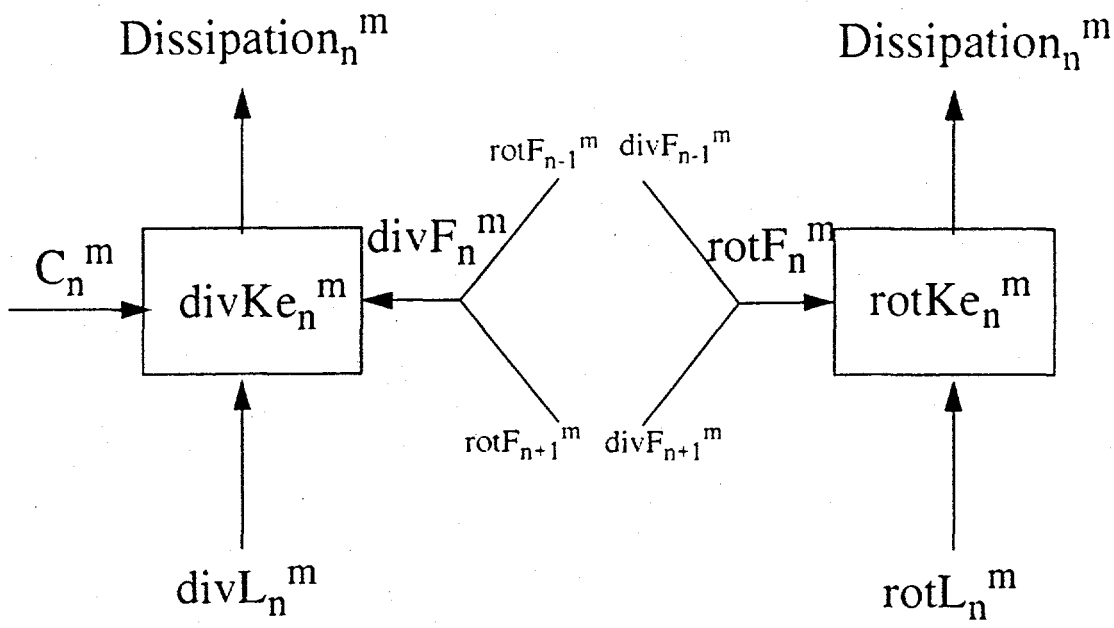

Figure 1. Schematic of the divergent / rotational kinetic energy budget (after Lambert, 1990).

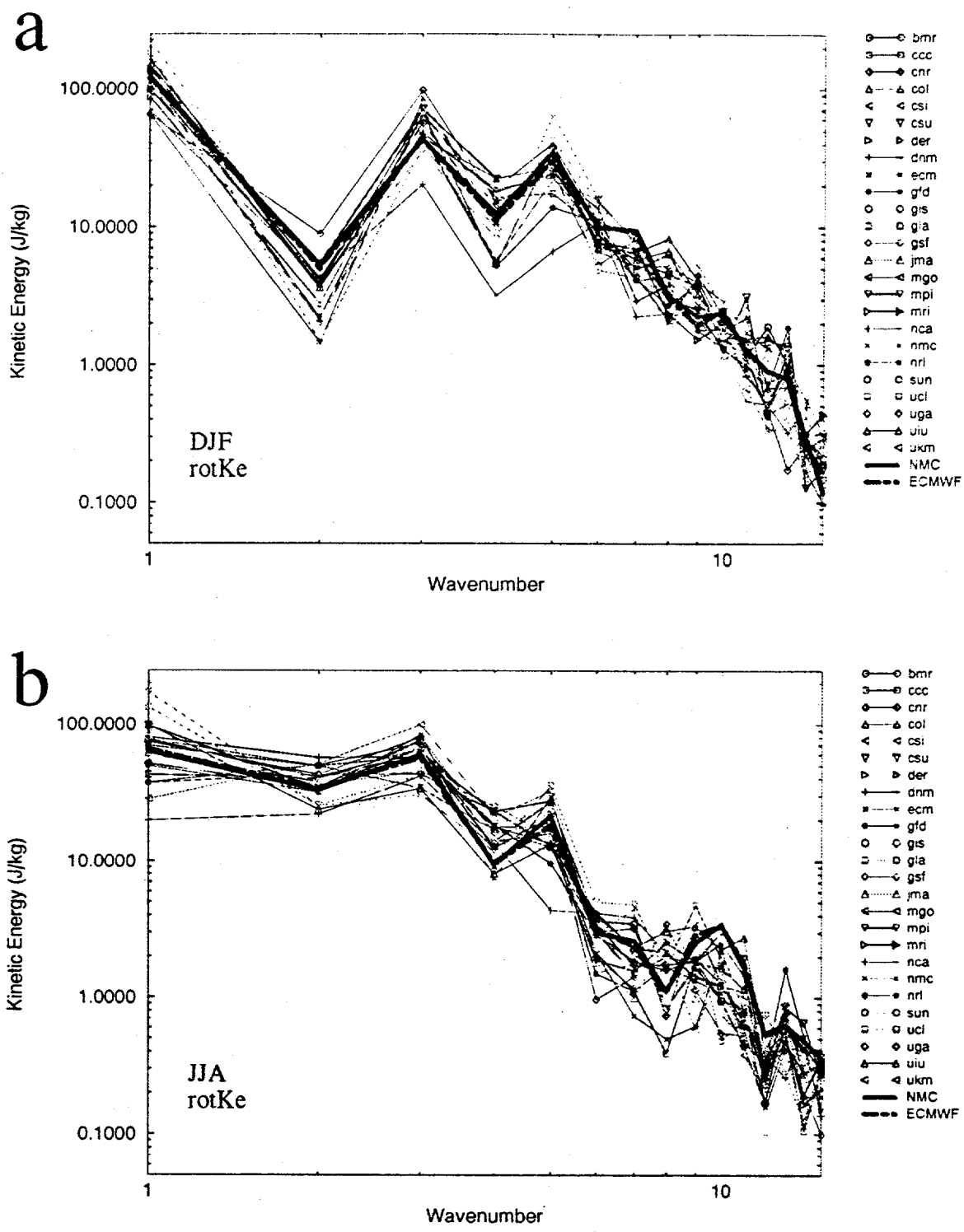

Figure 2. Rotational kinetic energy spectra at 200 hPa for (a) DJF and (b) JJA..

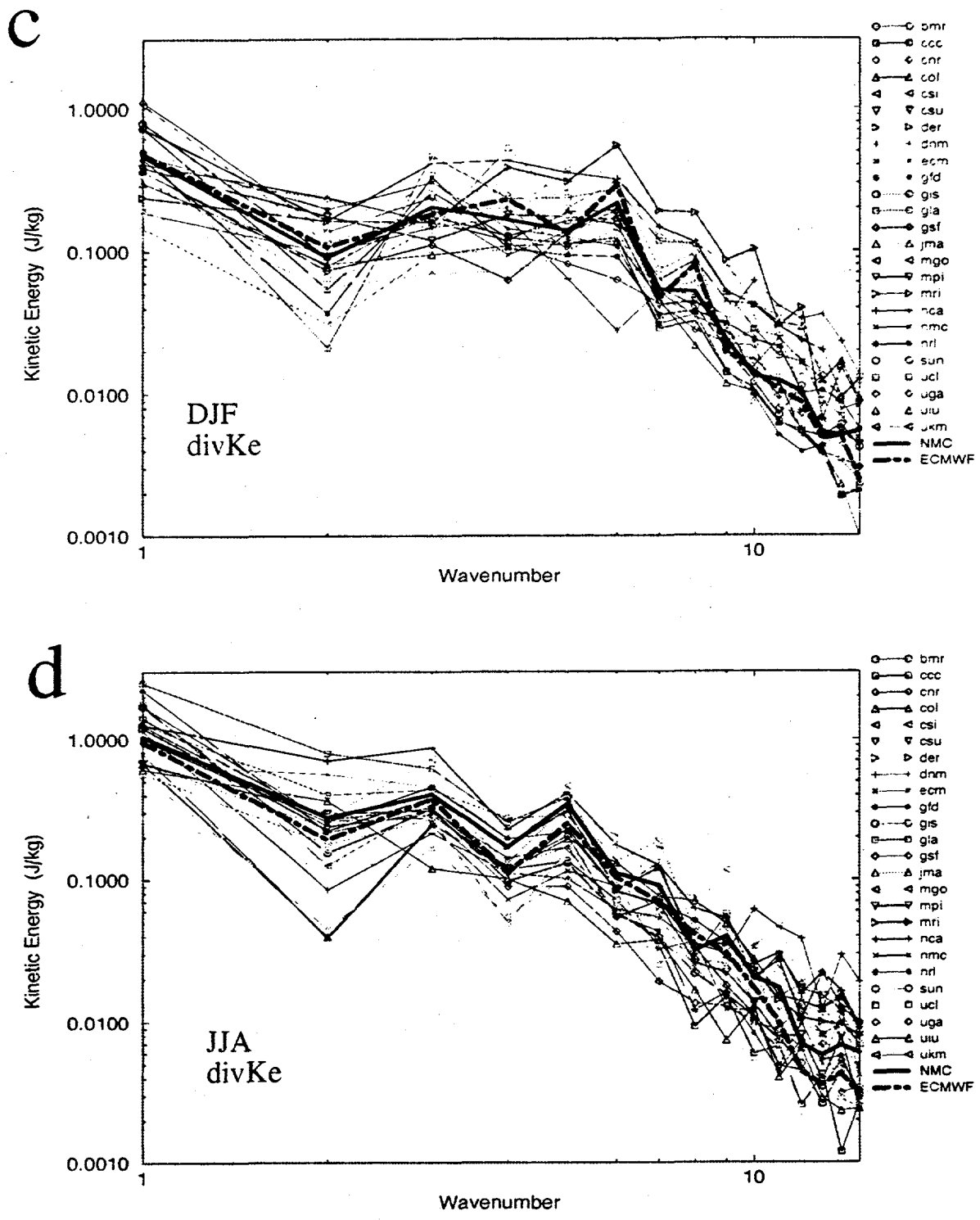

Figure 2 . Divergent kinetic energy at 200 hPa for (c) DJF and (d) JJA.

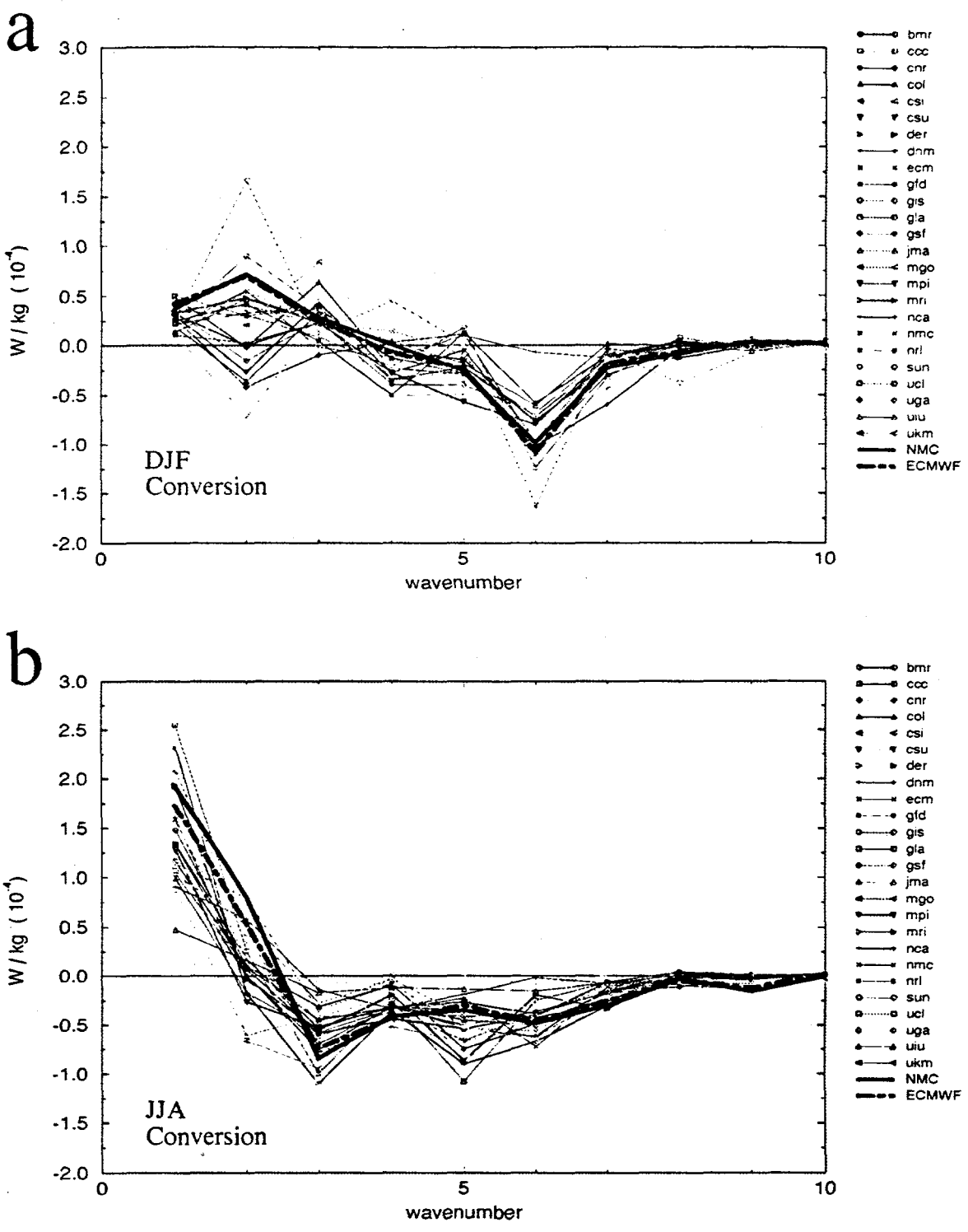

Figure 3 . Contribution to conversion term at 200 hPa for (a) DJF and (b) JJA

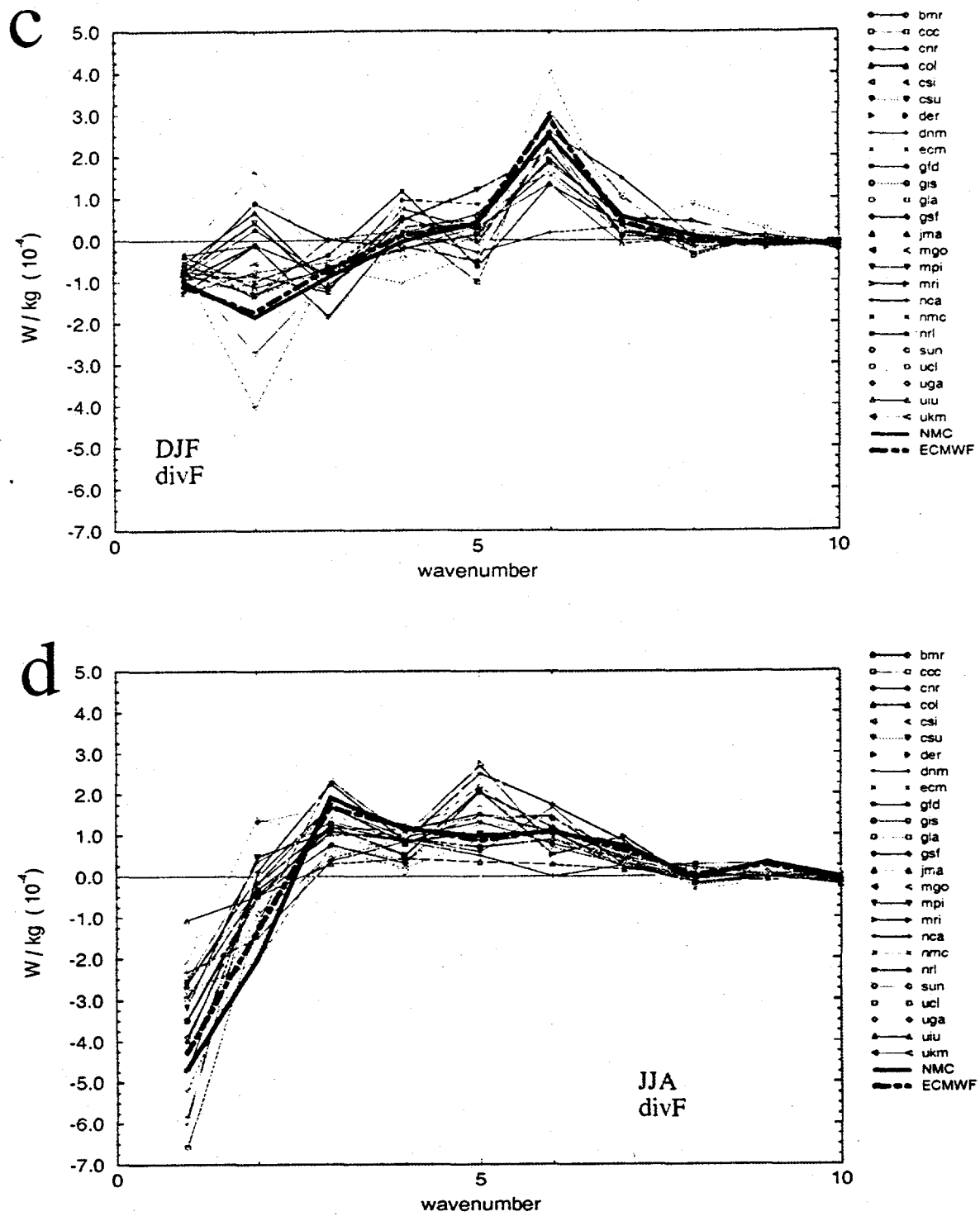

Figure 3. Contribution to divF at 200 hPa for (c) DJF and (d) JJA.

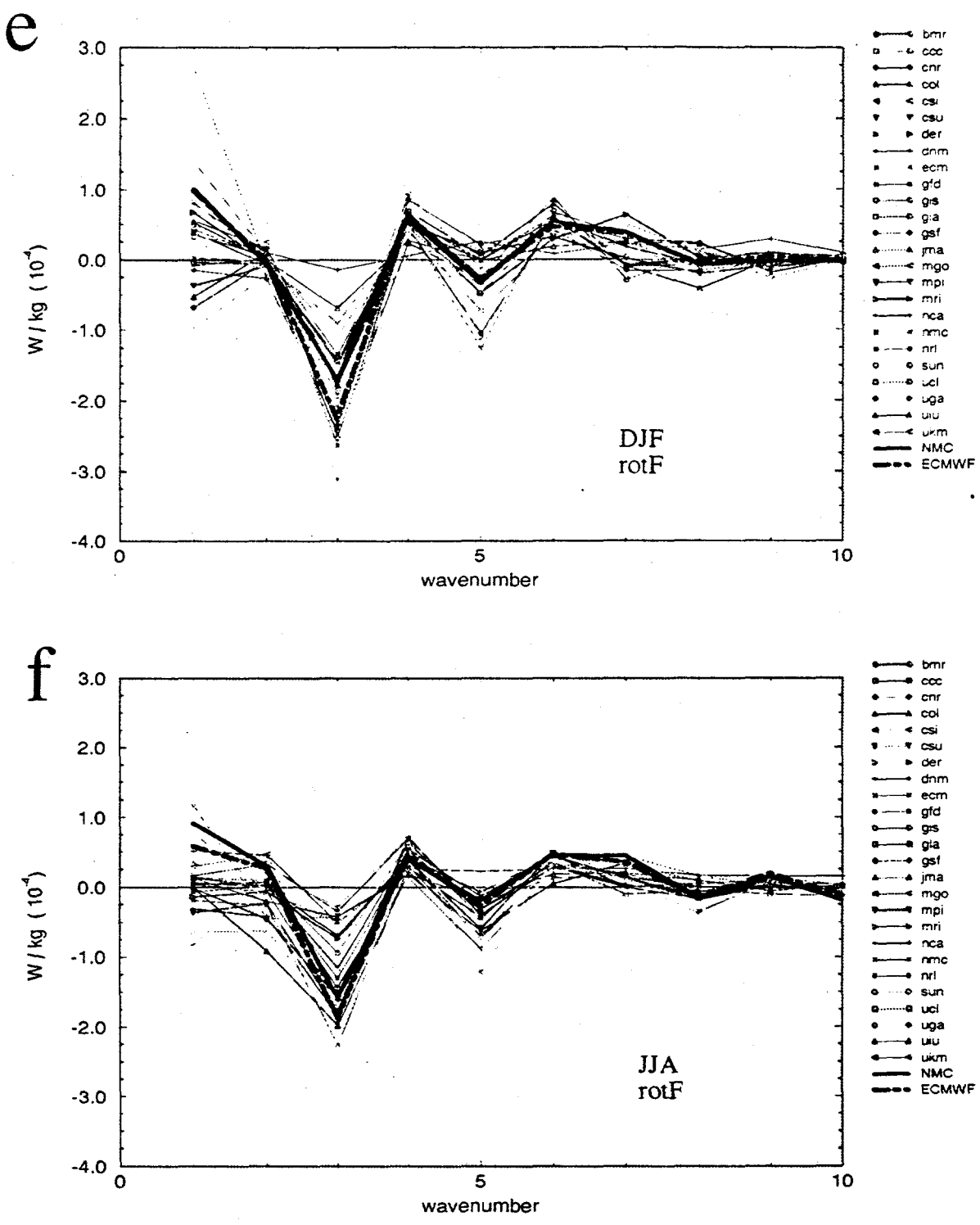

Figure 3. Contribution to rotF at 200 hPa for (e) DJF and (f) JJA.

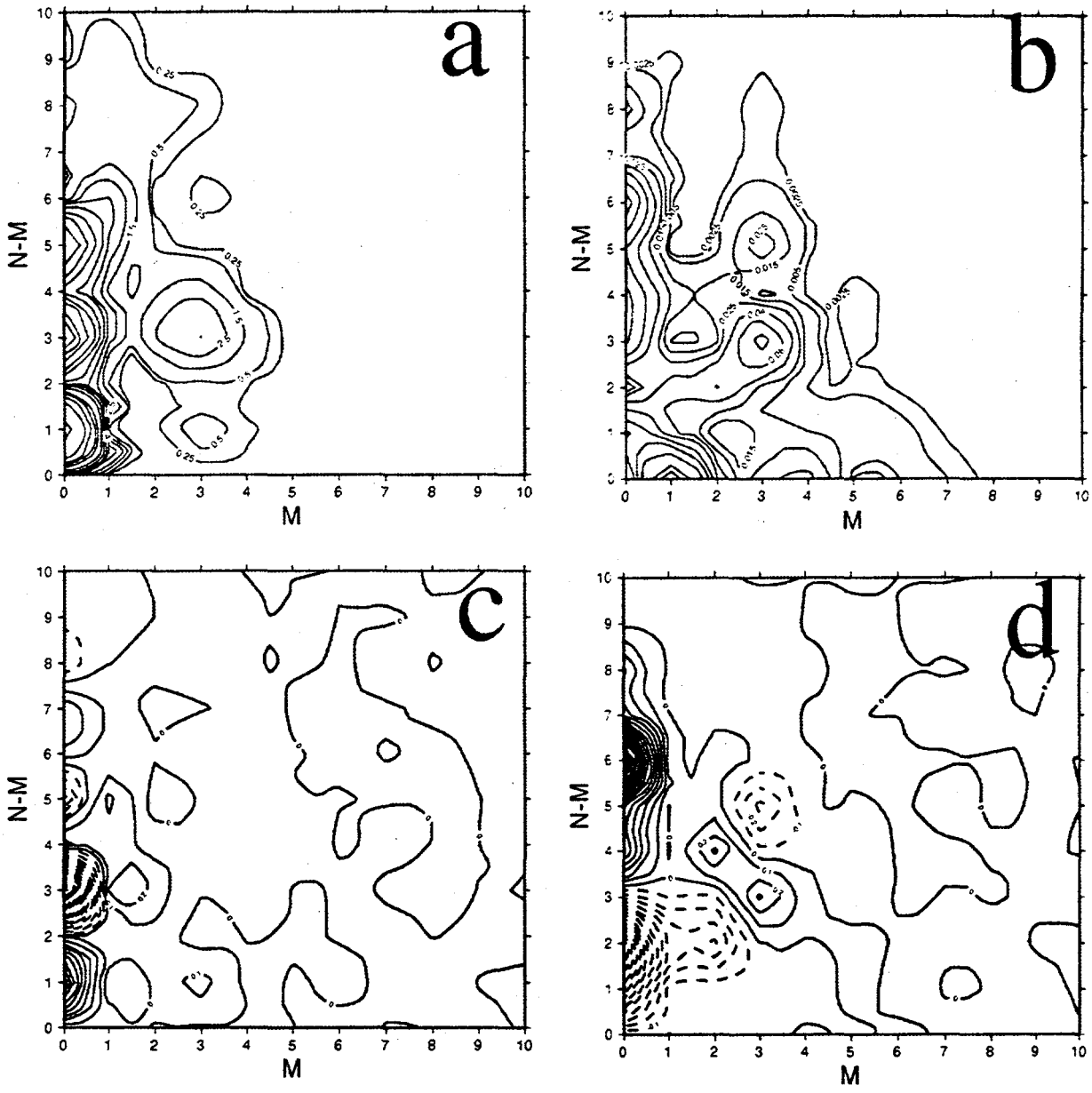

Figure 4 (a) The distribution of rotational KE for the ECMWF analysis for DJF in each two dimensional wave component. (b) As in (a) except for the divergent KE.(c) As in (a) except for the rotF (d) as in (a) except for the div. Contour interval is logarithmic.

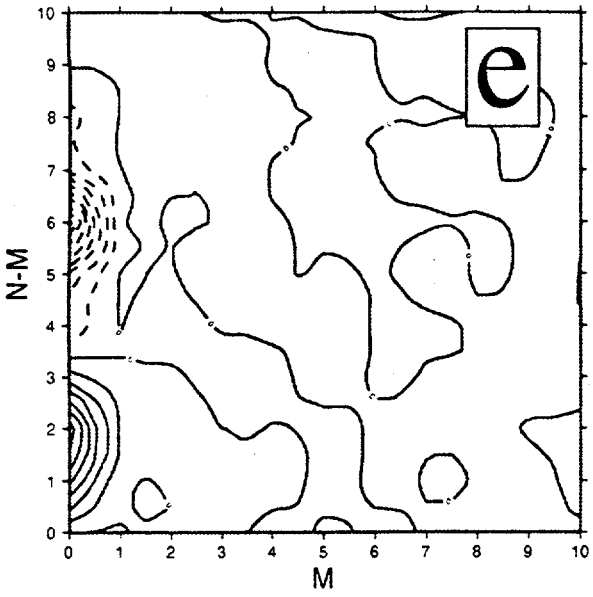

Figure 4. (d) As in (a) except for the conversion term.

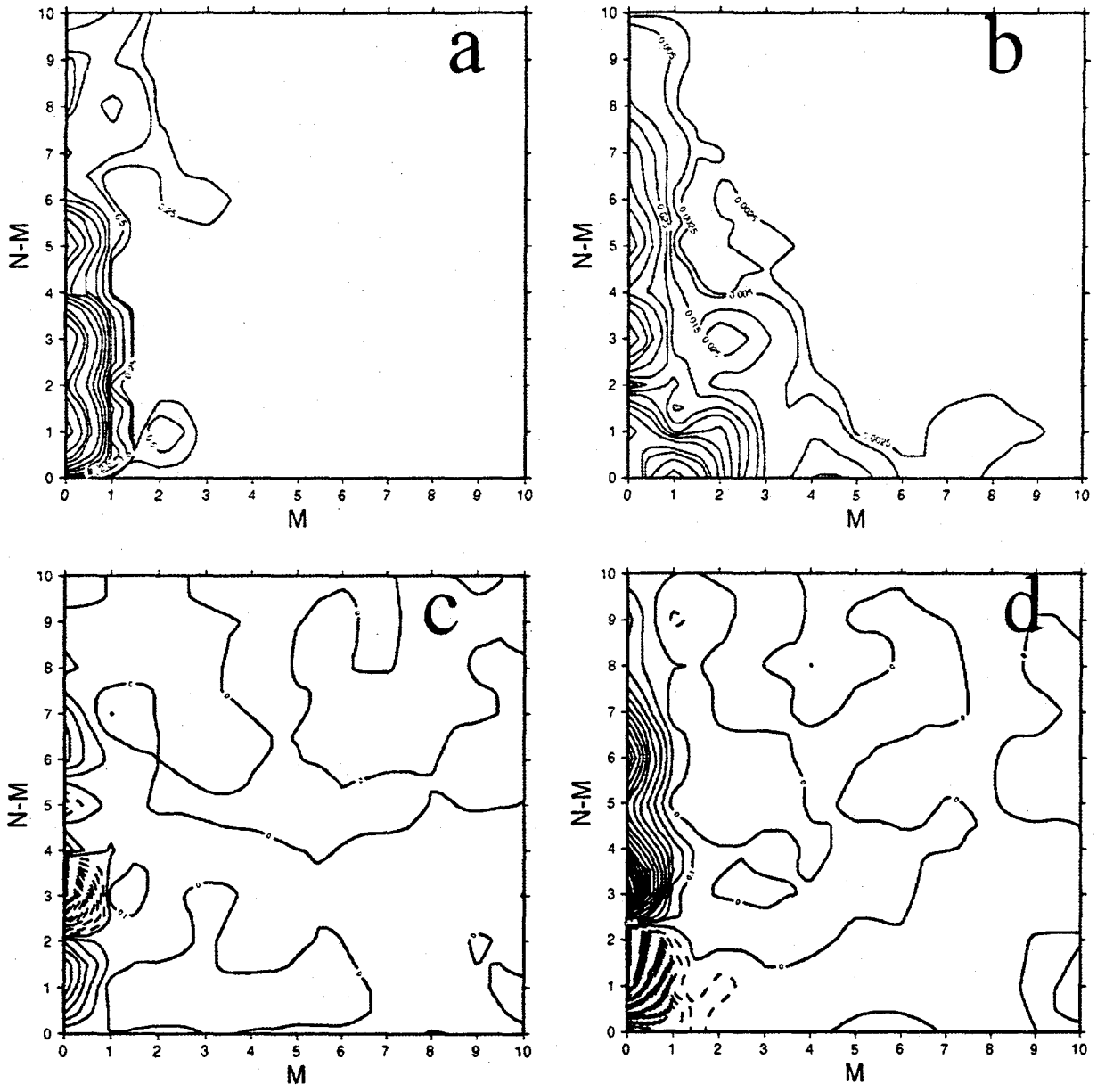

Figure 5. (a) The distribution of rotational KE for the ECMWF analysis for JJA in wavenumber space.

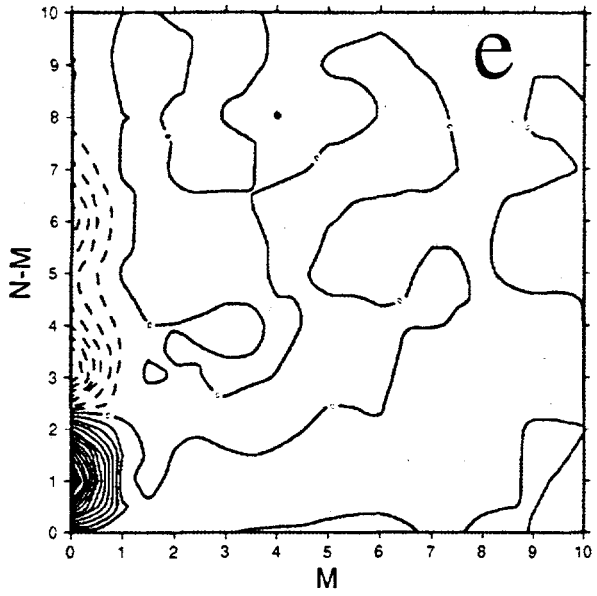

Figure 5 d. conv ECMWF JJA

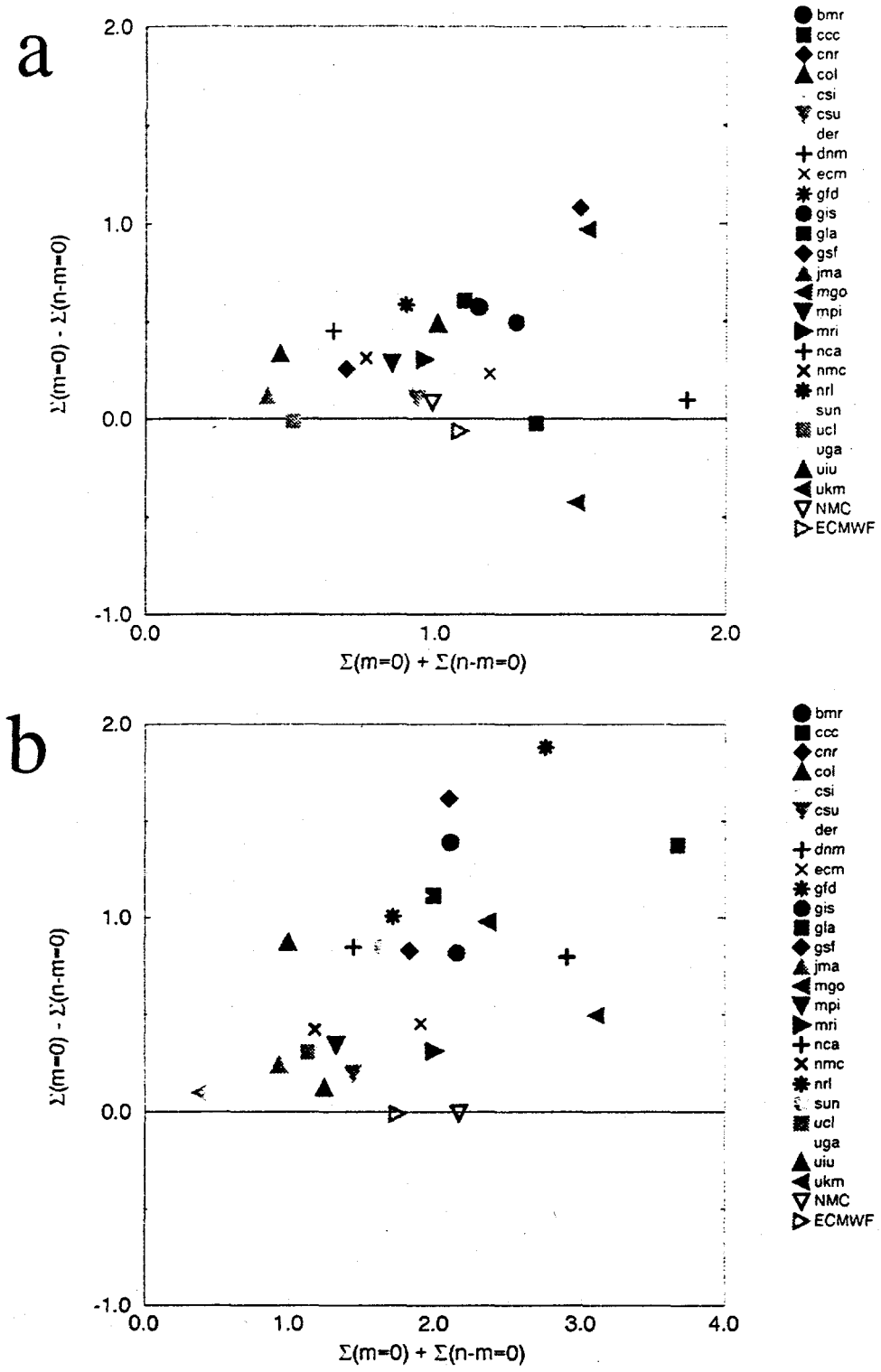

Figure 6 (a) DJF (b) JJA

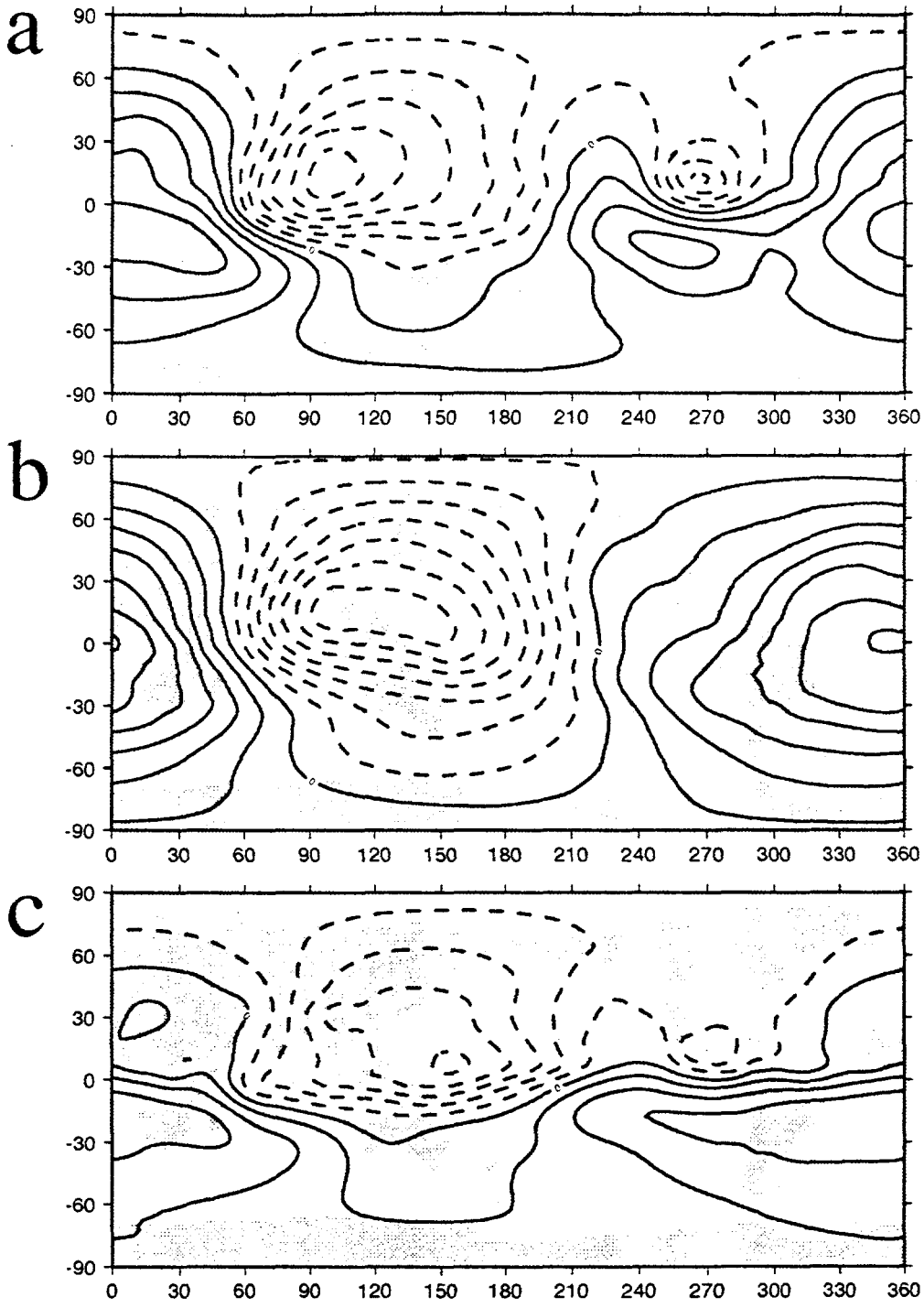

Figure 7. (a) ecm (b) cnr (c) uga

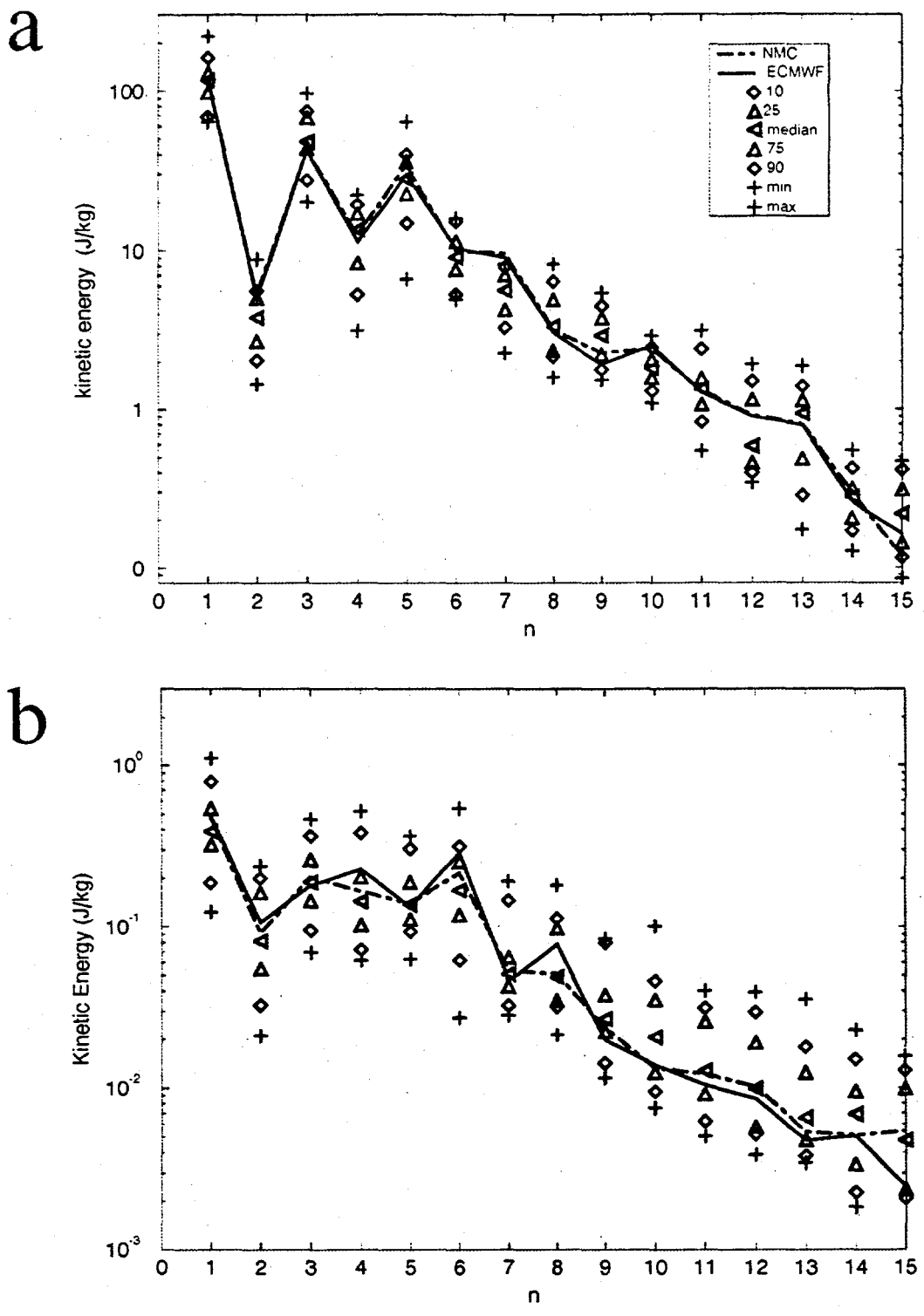
a
NMC
ECMWF
10
25
median
75
90
min
max
kinetic energy (J/kg)
100
10
1
0
0 1 2 3 4 5 6 7 8 9 10 11 12 13 14 15
n
b
Kinetic Energy (J/kg)
10^{0}
10^{-1}
10^{-2}
10^{-3}
0 1 2 3 4 5 6 7 8 9 10 11 12 13 14 15
n

Figure 8ab

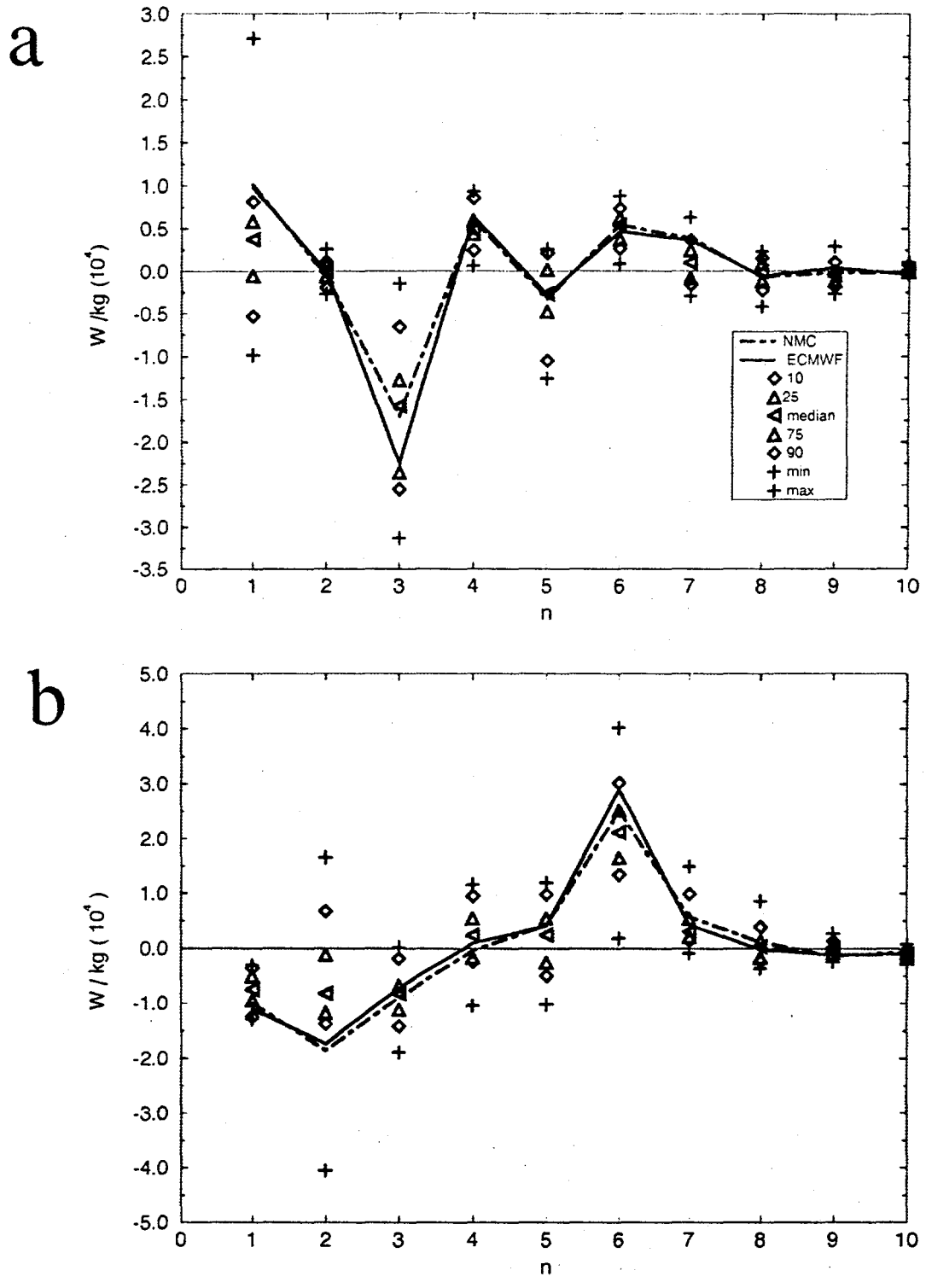

Figure 8 (c) and (d)

e

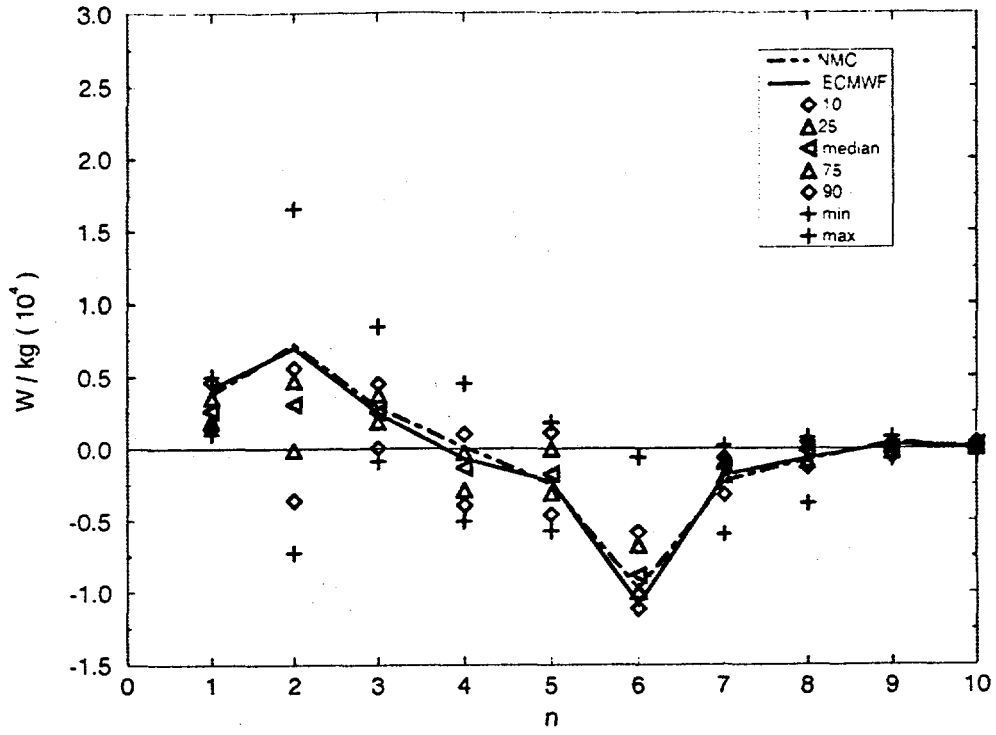
NMC
ECMWF
10
25
median
75
90
min
max
W / kg (10^4)
n
3.0
2.5
2.0
1.5
1.0
0.5
0.0
-0.5
-1.0
-1.5
0
1
2
3
4
5
6
7
8
9
10

Figure 8 e

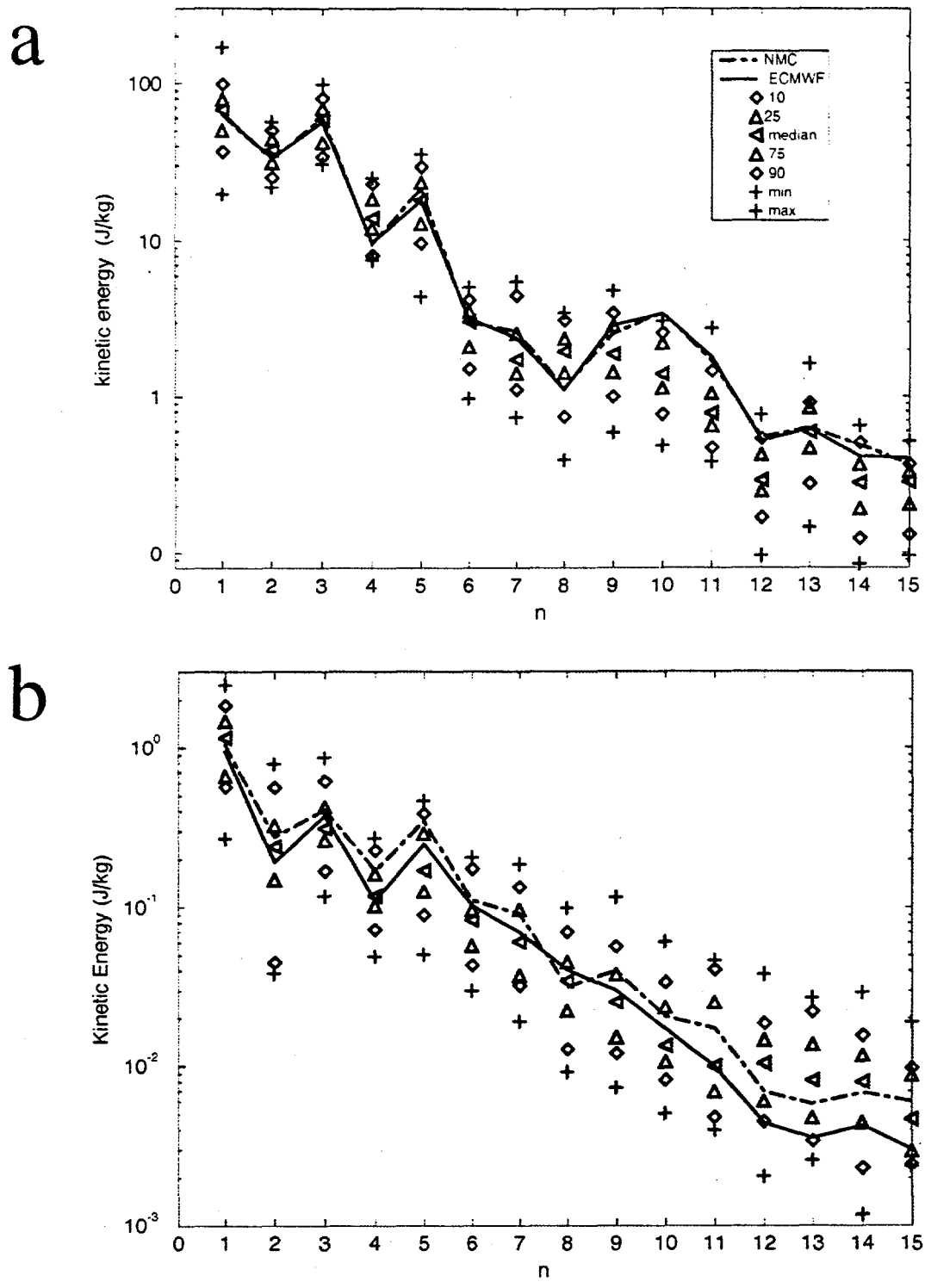

Figure 9 (a) rotKe JJA (b) divKe JJA

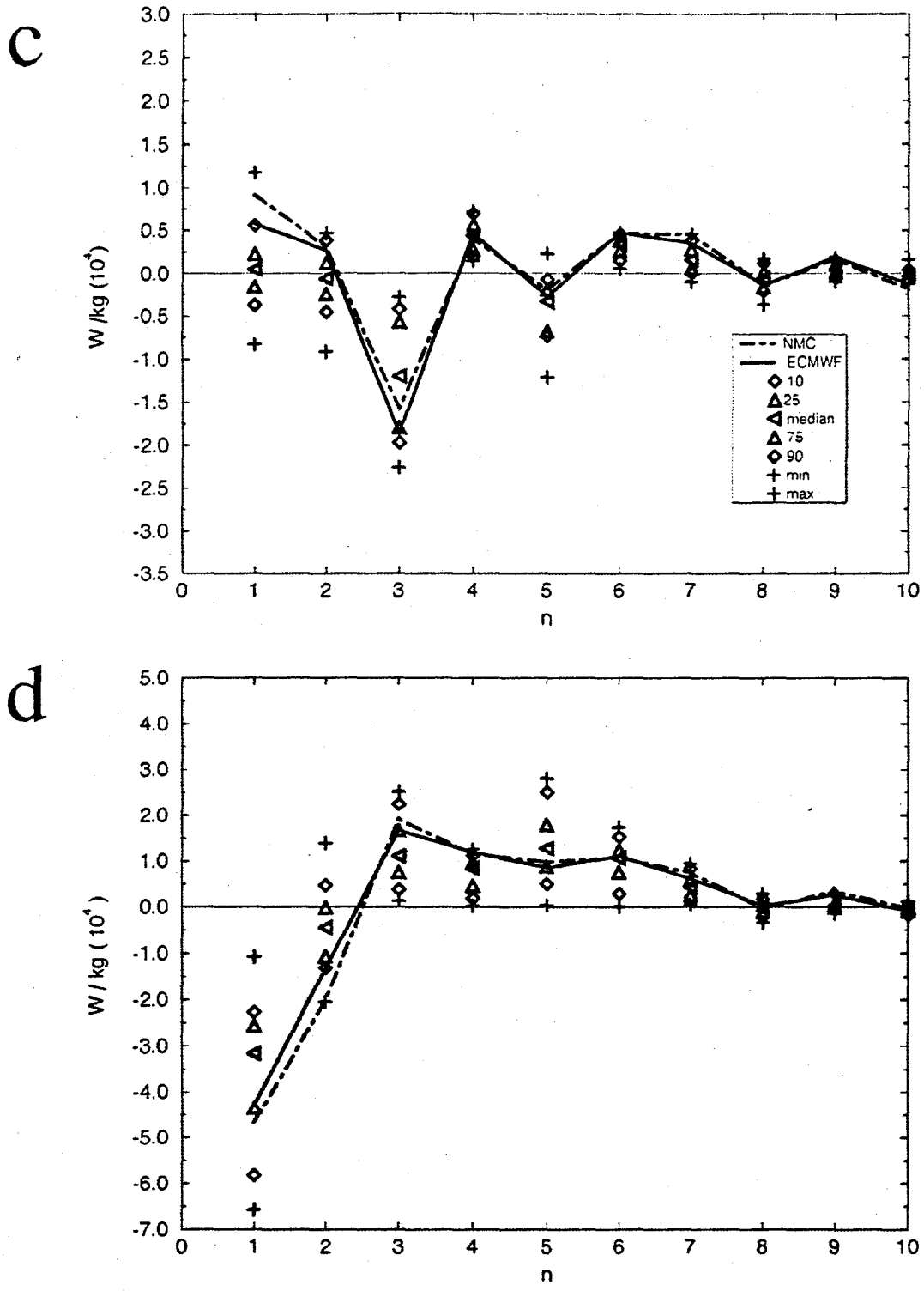

Figure 9 (c) rotF JJA (b) divF JJA

e

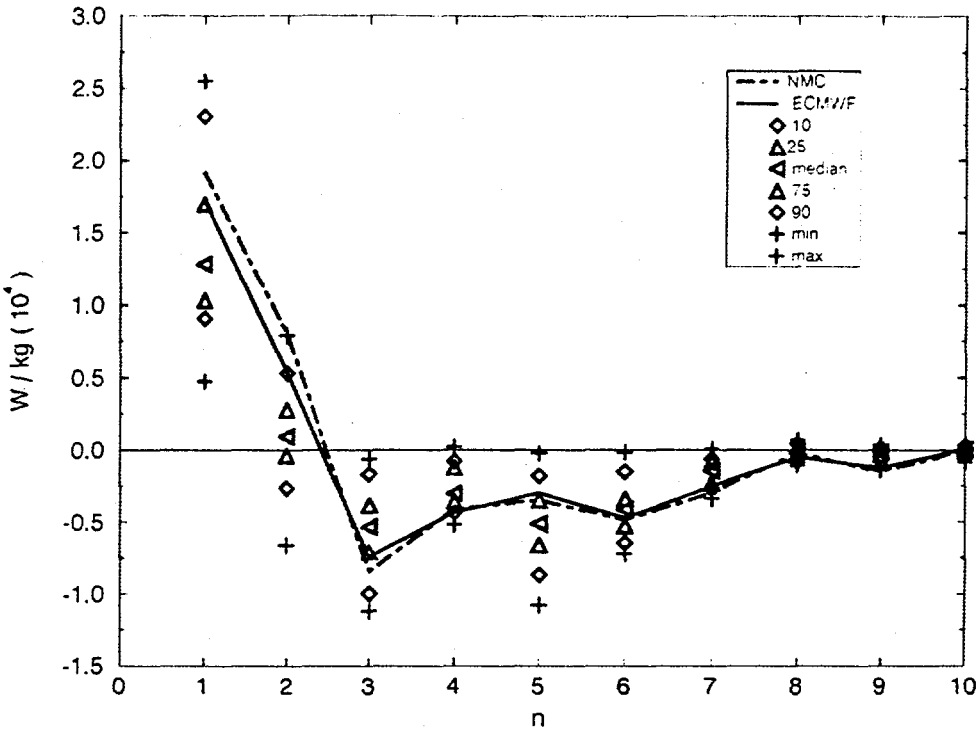
3.0
2.5
2.0
1.5
1.0
0.5
0.0
-0.5
-1.0
-1.5
W / kg (10⁴)
0
1
2
3
4
5
6
7
8
9
10
n
NMC
ECMWF
10
25
median
75
90
min
max

Figure 9 e

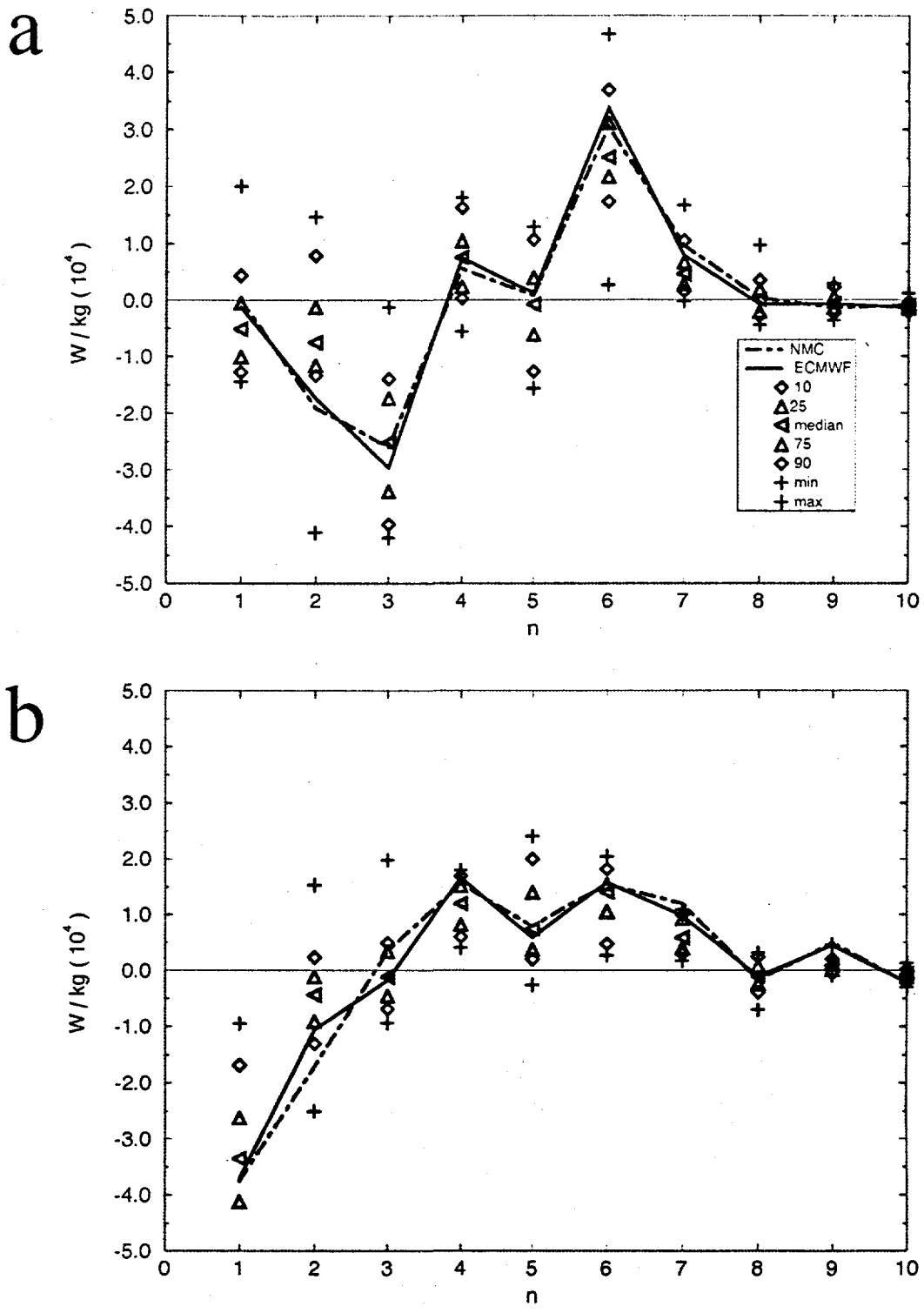

Figure 10 (a) totF DJF (b) totF JJA

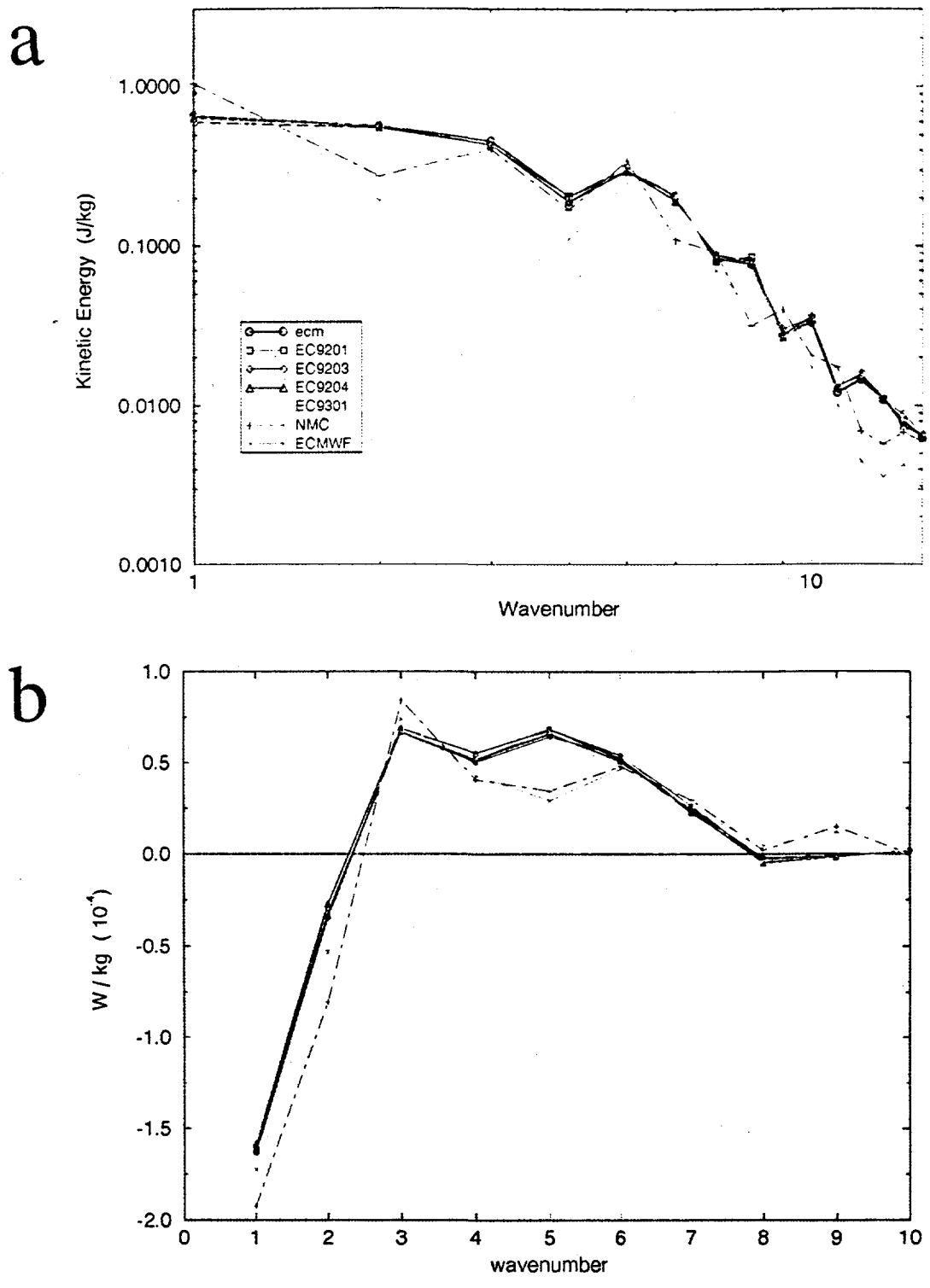

Figure 11 SENS (a) divKE JJA (b) conv JJA

PCMDI REPORTS

Number	Title	Author(s)	Date
1	The Validation of Atmospheric Model	W.L. Gates	March 1992
2	Analysis of the Temporal Behavior of Tropical Convection in the ECMWF Model	J.M. Slingo K.R. Sperber J.-J. Morcrette G.L. Potter	April 1992
3	The Effect of Horizontal Resolution of Ocean Surface Heat Fluxes in the ECMWF Model	P.J. Gleckler K.E. Taylor	July 1992
4	Behavior of an Ocean General Circulation Model at Four Different Horizontal Resolutions	C. Covey	August 1992
5	The Effects of Sampling Frequency on the Climate Statistics of the ECMWF General Circulation Model	T.J. Phillips W.L. Gates K. Arpe	September 1992
6	Sensitivity of Dynamical Quantities to Horizontal Resolution in a Climate Simulation with the ECMWF Atmospheric General Circulation Model (Cycle 33)	J.S. Boyle	October 1992
7	AMIP: The Atmospheric Model Intercomparison Project	W.L. Gates	December 1992
8	The Impact of Horizontal Resolution on Moist Processes in the ECMWF Model	T.J. Phillips L.C. Corsetti S.L. Grotch	January 1993

9	A Modeling Perspective on Cloud Radiative Forcing	G.L. Potter J.M. Slingo J.-J. Morcrette L. Corsetti	February 1993
10	The Use of General Circulation Models in Detecting Climate Change Induced by Greenhouse Gases	B.D. Santer U. Cubasch U. Mikolajewicz G. Hegerl	March 1993
11	Preliminary Validation of the Low Frequency Variability of Tropospheric Temperature and Circulation Simulated for the AMIP by the ECMWF Model	J.S. Boyle	April 1993
12	Simulation of the Indian and East-Asian Summer Monsoon in the ECMWF Model: Sensitivity to Horizontal Resolution	K.R. Sperber S. Hameed G.L. Potter J.S. Boyle	November 1993
13	Statistical Intercomparison of Global Climate Models: A Common Principal Component Approach	S.K. Sengupta J.S. Boyle	November 1993
14	Ocean Variability and its Influence on the Detectability of Greenhouse Warming Signals	B.D. Santer U. Mikolajewicz W. Brüggemann U. Cubasch K. Hasselmann H. Höck E. Maier-Reimer T.M.L. Wigley	January 1994

15	Cloud-Radiative Effects on Implied Oceanic Energy Transports as Simulated by Atmospheric General Circulation Models	P.J. Gleckler D.A. Randall G. Boer R. Colman M. Dix V. Galin M. Helfand J. Kiehl A. Kitoh W. Lau X.-Z. Liang V. Lykossov B. McAvaney K. Miyakoda S. Planton	March 1994
16	DRS User's guide	R. Drach R. Mobley	March 1994
17	The PCMDI Visualization and Computation System (VCS): A Workbench for Climate Data Display and Analysis	D.N. Williams R.L. Mobley	March 1994
18	A Summary Documentation of the AMIP Models	T.J. Phillips	April 1994
19	Global Ocean Circulation and Equator-Pole Heat Transport as a Function of Ocean GCM Resolution	C. Covey	June 1994
20	The Northern Wintertime Divergence Extreme at 200 hPa and Surface Cyclones as Simulated in the AMIP Integration of the ECMWF General Circulation Model	J.S. Boyle	November 1994

21	Towards the Detection and Attribution of an Anthropogenic Effect on Climate	B.D. Santer K.E. Taylor T.M.L. Wigley J.E. Penner P.D. Jones U. Cubasch	January 1995
22	The Effect of Horizontal Resolution on Cloud Radiative Forcing in the ECMWF Model	G.L. Potter	July 1995